Article

Corrosion Inhibition of Carbon Steel in a Sour (H₂S) Environment by an Acryloyl-Based Polymer

Muhammad Imran Ulhaq,* Qasim Saleem, Hassan Ajwad, Rashed M. Aleisa, Nayef M. Alanazi, Matteo Leoni, Ibrahim Zahrani, and Taras Makogon
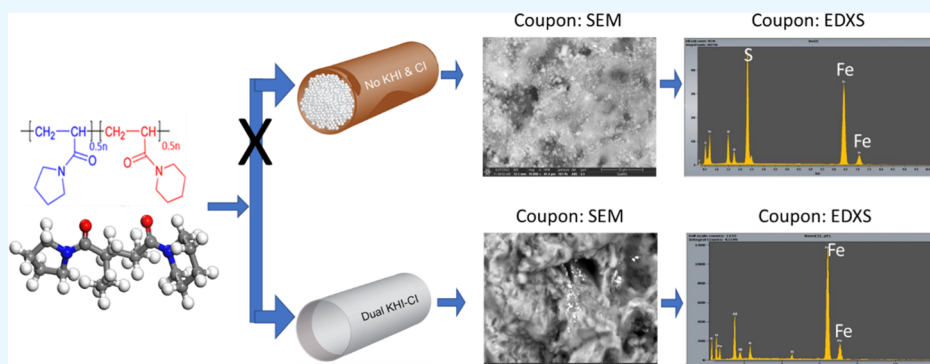
Read Online

ACCESS | Metrics & More | Article Recommendations | Supporting Information

ABSTRACT: Corrosion poses safety and operational challenges in the oil and gas field, particularly in a sour environment. Corrosion inhibitors (CIs) are thus employed to protect the integrity of industrial assets. However, CIs have the potential to dramatically impair the effectiveness of other co-additives, such as kinetic hydrate inhibitors (KHIs). Here, we propose an acryloyl-based copolymer, previously used as a KHI, as an effective CI. The copolymer formulation provided a corrosion inhibition efficiency of up to 90% in a gas production environment, implying that it can reduce or even eliminate the need for an additional dedicated CI in the system. It also demonstrated a corrosion inhibition efficiency of up to 60% under field-simulated conditions for a wet sour crude processing environment. Molecular modeling suggests that the enhanced corrosion protection is imparted by the favorable interaction of the heteroatoms of the copolymer with the steel surface, potentially displacing adhered water molecules. All in all, we show that an acryloyl-based copolymer with dual functionalities can potentially overcome issues caused by incompatibilities in a sour environment, resulting in significant cost savings and operational ease.

1. INTRODUCTION

Corrosion is a persistent flow assurance challenge in the oil and gas industry, accounting for more than 50% of pipeline failure and resulting in severe economic consequences and interruptions to operations, ecological pollution, safety hazards, and costly maintenance of pipelines.[1−3] Sour gas environments, characterized by the presence of elevated levels of hydrogen sulfide (H₂S), impart an additional source of concern due to the enhancing effect of the toxic gas on steel corrosion.[4]

Suitable corrosion inhibitors (CIs) are needed to mitigate the problem, especially in critical assets such as subsea pipelines. In practice, CIs are co-injected with other additives, such as kinetic hydrate inhibitors (KHIs), into subsea flow lines to protect the lines against corrosion caused by fluids that contain brine and acid gases (CO_2 and H_2S) while maintaining the gas flow.[5] However, the presence of corrosive gases in natural gas, such as H_2S and CO_2, causes the corrosion of steel-based pipelines.[6−8] Although H_2S corrosion is more severe than CO_2 corrosion, the most prevalent form of corrosion in the industrial sector is caused by CO_2-containing media.[9−11] In

contrast, a mixture of H_2S and CO_2 is highly corrosive to the steel during the production and transportation of oil and gas.[12] In addition, the presence of H_2S and CO_2 in hydrate deposits increases the rate of steel corrosion more than free gases. Moreover, during gas hydrate dissociation, a higher concentration of the gases is produced, intensifying the process of corrosion.[13]

Although CI and KHI usage prevents corrosion and gas hydrate formation, the simultaneous injection of CIs and KHIs, specifically, often results in incompatibility issues between both inhibitors.[14,15] CIs significantly reduce the performance of KHIs in most cases,[16] with reports of KHI performance

reduction of up to 50%.[17] This is attributed to the interference of the CI with the KHI's adsorption onto the gas hydrate surface.[18,19] At the same time, the performance of CIs is also reduced significantly in the presence of KHIs due to intermolecular interactions and preferred adsorptions of KHIs on the pipe wall or metal surface.[14−16,20] Many CIs are based on positively charged quaternary ammonium salts, which interact with carbonyl/amide groups of KHIs and reduce their performance. Some CIs based on anionic surfactants with excellent emulsifying or foaming properties accelerate gas hydrate formation.[21] Hence, KHI and CI incompatibility can potentially exacerbate hydrate formation in subsea flow lines.

Two possible paths are being explored to mitigate this risk: the development of ad hoc formulations containing the two inhibitors chosen to maximize compatibility and therefore performance[22] and the development of a single inhibitor exhibiting both KHI and CI functionalities.[5,14,23−27] The second approach to develop a single-molecule inhibitor with dual functions is of greater interest due to the reduction of cost and dosage realized when using one chemical instead of two inhibitors.[28] In recent years, ionic liquids, amino acids, biomolecules, and copolymers of vinyl caprolactam have been studied as dual-purpose KHCIs; however, their inhibition activity on gas hydrate has been undesirable, notwithstanding the high cost of some.[28] In addition, a number of researchers have reported new synthetic polymer/surfactant-based dual-purpose inhibitors including experimental and computational approaches to address the aforementioned cost and performance limitations.[29−34]

Recently, we proposed a new acryloyl-based copolymer KHI for sour environments with a high sub-cooling temperature of 8 °C, which is able to mitigate structure I-type gas hydrates.[35,36] Here, we demonstrate that such a material can also be used as an effective CI in a sour environment. Corrosion inhibition properties of the polymer were studied, which included electrochemical testing via linear polarization resistance (LPR), potentiodynamic polarization (PDR), and high-pressure high-temperature (HPHT) autoclave tests under field-simulated conditions for gas production and wet sour crude processing. A corrosion inhibition efficiency of up to 90% in a sour gas environment was observed, while maintaining a subcooling of 5.6 °C at ∼120 bars for 24 h. The polymer also demonstrated a corrosion inhibition efficiency of up to 60% under field-simulated conditions for a wet sour crude. These results highlight a path toward developing a single formulation that exhibits both corrosion and gas hydrate inhibition, specifically for sour environments.

2. EXPERIMENTAL PROCEDURE

2.1. Materials. All chemicals were purchased from Sigma-Aldrich and used as received, acryloyl chloride (97%), pyrrolidine (99%), piperidine (99%), trimethylamine $(CH_3)_3N$ (97%), 4,4′-Azobis (4-cyanovaleric acid) (98%), thioglycolic acid (98%), diethyl ether (99%), methanol (99%), monoethylene glycol (MEG, 97%), and deuterated solvents $(D_2O$ (99.9%) and $CDCl_3$ (99.8%)). All water used was of Milli-Q quality.

2.2. Synthesis and Characterization of the Copolymer. The acryloyl-based copolymer employed in this work is shown in Figure 1. Detailed synthesis and characterization using nuclear magnetic resonance (NMR) and gel permeation chromatography have been published.[36,37] Additional material properties of the copolymer and further analytical studies using
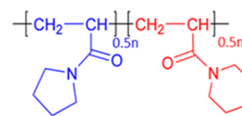

Figure 1. Structure of the acryloyl-based copolymer.

FT-IR, TGA, and DSC are included in the Supporting Information.

The proposed inhibitor is formulated as a solution of the copolymer of a molecular weight of ∼1000 Da in different solvents depending on the testing method (see Table 1). The terms copolymer and KHCI (dual-purpose corrosion and kinetic hydrate inhibitor) are used in the Results and Discussion section to refer to the polymer itself or the formulation in which the copolymer is the active ingredient, respectively.

2.3. Thermal Stability. The developed formulation was tested at three different temperatures (25, 50, and 90 °C) to assess thermal stability. The material was heated to the target temperature and then held for 5 min for the stability assessment. The assessment included visual examination or appearance before and after the test to ensure integrity (phase separation, decomposition, color change, and precipitation formation).

2.4. Corrosion Inhibition Testing. Electrochemical and autoclave tests were carried out using the copolymer or KHCI for different applications.

2.4.1. Linear Polarization Resistance. The LPR measurement was conducted on a C-1018 mild carbon steel coupon (surface area of 9 cm^2) in 3.5% NaCl solution at 60 °C using ASTM method G59-97. The CO_2 gas was purged at a constant rate of 25 mL/min during the exposure time for the test. The experimental setup consists of a corrosion cell connected to a potentiostat (PARSTAT 4000 from Ametek Scientific Instruments). The LPR measurements were carried out using a glass setup with a volume capacity of 0.85 L. The carbon steel coupon-exposed surface area (9 cm^2) was used to measure the corrosion for 24 h.

An initial 50 ppm of the copolymer was injected to the testing mixture after a stable baseline. After 4 hours from the first injection, another injection of 50 ppm of the copolymer was performed, and the corrosion rate was observed until the end of the experiment. Data acquisition was completed via software that enables the measurement of corrosion rate.

2.4.2. Potentiodynamic Polarization (PDP). The above-mentioned experimental parameters for LPR testing were used here as well. In addition, PDP measurements were performed using a conventional three-electrode cell, where the carbon steel was the test electrode, with a saturated calomel electrode as a reference electrode and platinum as the counter electrode. Prior to starting the PDP scans, the test electrode was allowed to stabilize for approximately 60 min. Immediately following the stabilization period, the test electrode was polarized at a scan rate of 1.66 mV/s from an initial potential of −1 V (vs OCP) to a final potential of +1 V. The corrosion potential (E_{corr}), corrosion current density (I_{corr}), and anodic/cathodic Tafel slopes (βA and βC) were calculated from these tests using CorrWare software (Scribner Associates Inc.). Then, based on the approximate linear polarization at E_{corr}, polarization resistance (Rp) values were determined.

2.4.3. Autoclave Testing under Field-Simulated Conditions. HPHT corrosion tests were performed on similar C-

Table 1. Details of Samples and Formulations Used for Different Compatibility and Performance Evaluation Tests

formulation components	electrochemical testing	thermal stability	rocking cell (KHI)	gas production test-1 (HPHT)	crude processing-(HPHT)	gas production test-2 (HPHT)
1	copolymer	copolymer (35%)	copolymer (35%)	copolymer (35%)	copolymer (10%)	copolymer (35%)
2		MEG (65%)	MEG (65%)	MEG (65%)	imidazoline (5%), surfactant-1%	MEG (65%)
3					water (85%)	

Table 2. Detailed Experimental Conditions for Performance Evaluation of the Formulation as Corrosion Inhibitors Using the HPHT Autoclave for Different Applications

field condition application	water geochemical analysis, mg/L		operational conditions		gas composition, mole %		time (h)	RPM	KHCI conc. (ppm)
			pressure (Psig)	temp. (°C)					
gas production test-1	Cl	607	1600	90	CH_4	79.6	24	500	2500 and 10,000
	Na	393			CO_2	9.2			
	acetic acid	500			N_2	7.2			
	formic acid	250			H_2S	2.3			
	TDS	1750			ethane	1.4			
	pH	6.5			propane	0.2			
					n-butane	0.1			
sour crude processing	Na	29,500	250	83	CO_2	7	24	400	20 & 100
	Ca	8210			N_2	90			
	Mg	1080			H_2S	3			
	Cl	61,800							
	SO_4	1300							
	HCO_3	662							
	TDS	102,552							
	pH	6.6							
gas production test-2	Na	29,500	1600	90	CH_4	79.6	42	500	2500
	Cl	61,800			CO_2	9.2			
	acetic acid	500			N_2	7.2			
	formic acid	250			H_2S	2.3			
	TDS	1750			ethane	1.4			
	pH	6.6			propane	0.2			
					n-butane	0.1			

1018 steel coupons using a 4 L rotating autoclave vessel. The test conditions are chosen as close as possible to the field conditions already proposed in Table 2. Note that the experimental time difference stems from the fact that two different tests (1 and 2) and different testing protocols were used as approved for testing conditions.

A rotating cage apparatus was employed to generate controlled dynamic (flow) conditions inside the reactor. The steel coupons were cleaned and degreased before and after testing. The coupons were positioned in a fixed cage made of PEEK and then mounted in the autoclave. A total of eight coupons were mounted in each run: four coupons fully immersed in the water phase and the other four coupons mounted in the gas phase. The pre-deaerated test media was then introduced to the autoclave vessel. Deaeration was accomplished by a 2 h purge with nitrogen gas in an externally sealed container. The vessel was then closed, and all necessary connections were primed to start the test. The test solution (low TDS water) was transferred to the autoclave under oxygen-free conditions followed by 3 pressure/de-pressure cycles with nitrogen to further ensure oxygen removal. The shaft rotation was set at 500 rpm. The system was then heated to a target temperature of 90 °C. Upon reaching the target temperature, the autoclave was pressured with the gas mixture

to 1600 psi (110 bars). The test conditions were monitored throughout the test duration.

Upon completion of the tests, the autoclave was allowed to cool down to room temperature. The test coupons were unscrewed from the rotating cage, visually inspected, and photographed. The coupons were cleaned as per the procedure and re-inspected again. The corrosion rate and inhibition efficiency of the test sample (KHCI) were calculated using the weight loss by eqs 1 and 2, respectively

$$\text{corrosion rate (CR) (MPY)} = \Delta W^* 22{,}300/D^* A^* T \qquad (1)$$

where ΔW is the weight loss of the coupon in mg, D is the density of C-1018 steel (7.86 g/cm³), A is the area of the exposed coupon (5.66 in²), and T is the exposure time (one day). The MPY unit means mils per year.

$$\text{inhibition efficiency (IE \%)}$$
$$= (CR_{blank} - CR_{inhibitor})^* 100/CR_{blank} \qquad (2)$$

2.5. Rocking Cell Performance Evaluation. The performance of the formulation as the KHI was confirmed using a slightly modified procedure from the literature.[37] The formation of natural gas hydrates produced from a field was simulated in the rocking cells (PSL System Technik, Germany). The RC-5 consists of five Hastelloy cells capable

of operating under high pressure (maximum 200 bar) and sour gas conditions. The Hastelloy cells are immersed in a temperature-controlled bath containing ethylene glycol. During operation, the RC-5 is rocked using a mixing ball, which slides along the length of each Hastelloy cell to ensure that the reactant slurry is well mixed. The volume of each Hastelloy cell with the mixing ball was 30 mL. The RC-5 enables the formation of a gas hydrate under simulated operating conditions to test KHI effectiveness. Data acquisition, pressure and temperature with time for each Hastelloy cell, is carried out with WinRC software.

In a typical run, each of the Hastelloy cells was charged with KHCI (Table 1), 10 mL of synthetic brine, and a field synthetic gas at ~120 bars and 21 °C. After the reactant composition was fixed, the RC-5 temperature was programmed to change in 3 stages, as presented in Table 3. Each

Table 3. Temperature Program to Form Natural Gas Hydrate in the RC-5

stage	start temp (°C)	average ramp (°C/min)	T_{sc} (°C)	duration (min)
S-1	14.6	0.1	4	7240
S-2	13.0	0.1	5.6	7240 to 8680
S-3	8.0	0.08	10.5	8680 to 8800

temperature (after the first at 21 °C) is selected to be in a stable gas hydrate region. The 3-phase equilibrium (i.e., liquid, vapor, and hydrate) was calculated with the HYSYS program to be 18.6 °C at 140 bar. The sub-cooling temperature (T_{sc}) was defined as the difference between the operating temperature and the 3-phase equilibrium temperature at 140 bar. By accurate monitoring of the pressure of the cell, information about natural gas hydrate formation can be obtained. In parallel to monitoring the pressure, changes in pressure associated with vapor, liquid, and natural gas hydrate phases were considered using a mass balance of the field natural gas so that pressure changes can be accurately attributed to natural gas hydrate formation. The duration of subcooling stages is prolonged compared to the previously published procedure, as mentioned above.[37] A passing criterion that results of 2 out of 2 cells should be consistent was set to ensure reproducibility.

The composition of the synthetic gas and brine used in the experiments is given in Table 4.

Table 4. Synthetic Gas and Brine Composition

gas component	mole %	brine species	concentration (mg/L)
nitrogen	7.2	chloride	607
carbon dioxide	9.2	sodium	393
hydrogen sulfide	2.3	acetic acid	500
methane	79.6	formic acid	250
ethane	1.4	TDS	1750
propane	0.2		

2.6. Computational Modeling. In order to capture the full complexity of the material, a wide set of random oligomeric copolymers would need to be generated and simulated. This would, however, still not guarantee exploration of the whole space of configurations. As an alternative, often met in the literature, dimers representing the local environment along the polymeric chain are studied. In this case, considering the copolymeric nature of the material, the AB dimer (where A

and B are the two comonomers of Figure 1) was studied as a representative for the system. This would allow for a homogeneous direct comparison with existing literature data on different systems.

Molecules were designed in BIOVIA Materials Studio 2017 software (Dassault Systemes, Waltham, MA, USA) and automatically completed with hydrogens. Methyl groups were used to cap the open ends of the dimer. For the subsequent calculations, several modules of software were used. Extensive geometry search over the full torsional range was performed using the Conformer module and the COMPASS forcefield to find lowest-energy configuration candidates. The geometry of the lowest energy conformers was further optimized using DFT by means of the DMol³ module. The hybrid B3LYP functional was employed to improve the accuracy of the result. The conductor-like screening model (COSMO) with a dielectric constant of 78.54 was used to simulate the effect of water solvation.

The adsorption energies of the molecules on the steel surface were obtained using the adsorption locator module. The Metropolis Monte Carlo methodology was used as reported earlier.[38,39] To simulate the ferritic C-1080 steel, a bulk *bcc* Fe crystal was imported from the software database and cleaved into the most stable *bcc* Fe (110) surface with a slab thickness of 5 Å. Finally, a 10 × 10 supercell with periodic boundary conditions and a vacuum thickness of 30 Å was constructed. The optimized KHCI molecules were placed onto Fe (110) surface in a simulation box in the presence of 200 water molecules to simulate the effect of the aqueous environment. Simulated annealing was then employed to optimize the system using the COMPASS forcefield and to obtain the molecular configurations as well as adsorption energies of the chosen molecules and of water.

3. RESULTS AND DISCUSSION

3.1. Material Properties of the Formulation. The KHCI exhibited excellent stability at three distinct temper-

Table 5. Thermal Stability of the KHCI Sample

Properties of KHCI	Temperature (°C)		
	25 °C	50 °C	90 °C
Appearance			
Color	No change	No change	No change
Precipitation	No	No	No
Phase separation	No	No	No

atures (25, 50, and 90 °C): no phase separation, color change, or precipitation were detected (see Table 5).

The acryloyl-based copolymer used in the KHCI tends to precipitate out of solution above the so-called lower critical solution temperature (LCST), a parameter that is dependent on polymer concentration, molar composition of monomers, and the solvent/additives present.[40] The critical concentration to achieve the minimal LCST of similar copolymers in solution is 1.5%,[40] which is much higher than the concentrations employed in the field for this particular copolymer. Indeed, at a lower concentration, severe aggregation and precipitation of the polymer were not observed as measured via ¹H NMR spectroscopy (Figure S2). Other thermal properties of the copolymer were also explored via TGA and DSC and are
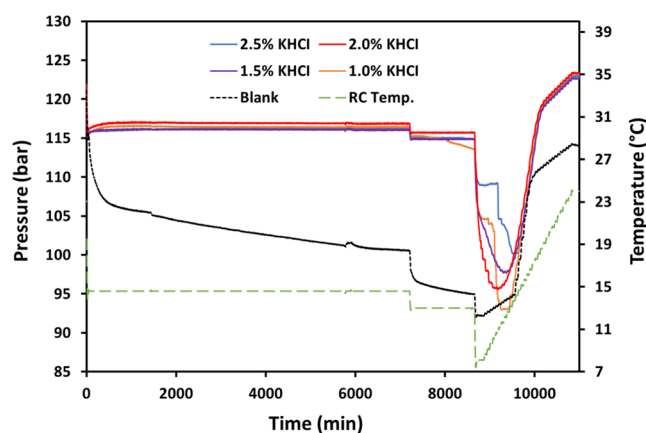
Figure 2. Rocking cell data of formulation at different dosage rates (1, 1.5, 2.0, and 2.5%).

Figure 4. Potentiodynamic polarization curves for corrosion test in NACE brine at 60 °C with 100 ppm (dotted line) and without (solid line) the copolymer.

reported in the Supporting Information (Figures S3 and S4, respectively).

3.2. Performance of Formulation as KHIs. The performance evaluation results of the copolymer used in this report as KHIs are presented in Figure 2. The test was carried out at four different dosages (2.5, 2.0, 1.5, and 1.0 wt %) as a formulation with monoethylene glycol (MEG).

For all chosen dosages, the formulation delayed the hydrate nucleation at a T_{sub} of 4.0 °C (1st subcooling) for 5 days. The sharp drop in pressure within the first hour for the blank sample indicated the formation of gas hydrate. No hydrate formation was observed at a T_{sub} of 5.6 °C (2nd subcooling) for 1 day under all dosages. A significant drop in pressure was observed at a T_{sub} of 10.0 °C (3rd subcooling) for lower dosage compared to a higher dosage of the KHCl. Hence, a higher dosage of the KHCl (>2.5%) could achieve a T_{sub} larger than 5.6 °C for S-I type hydrate in a sour (H_2S) environment.

3.3. Corrosion Inhibitor Performance Evaluation of the Copolymer/KHCl. *3.3.1. Linear Polarization Resistance.* The LPR can be used to obtain accurate instantaneous information about the corrosion rate of the metal with time. The initial corrosion rate baseline of C-1018 (without the copolymer) was around 200 mpy. After a total injection of 100 ppm of the copolymer, the corrosion rate dropped to 20 mpy, as shown in Figure 3A. The inhibition efficiency (IE), calculated from the corrosion rate plot, was around 90% (Figure 3B), indicating the high corrosion inhibition potency of the copolymer.
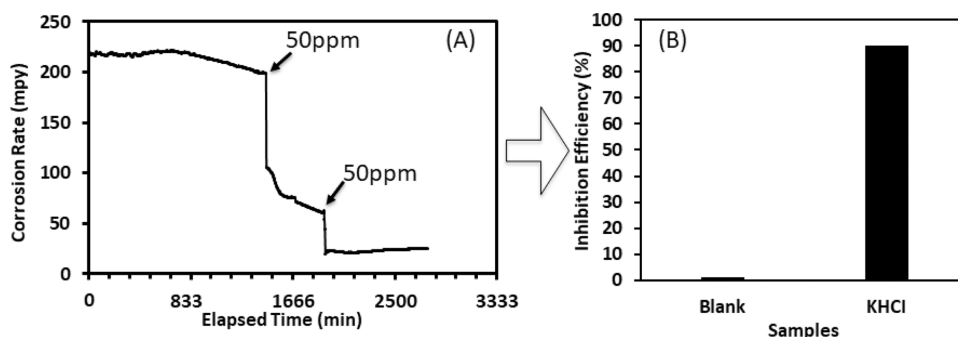
3.3.2. Potentiodynamic Polarization (PDP). The potentiodynamic polarization curves with and without copolymers are shown in Figure 4. The anodic curve confirms the high performance of the copolymer, as the corrosion potential of the sample tested with the inhibitor is higher than the blank. The corresponding electrochemical properties, including the corrosion inhibition efficiency (IE) and the surface coverage, are listed in Table 6. Inhibition efficiency and surface coverage were calculated using eqs 3 and 4, respectively.

$$IE\ (\%) = (I_{corr}^{\circ} - I_{corr}/I_{corr}^{\circ}) \times 100 \tag{3}$$

$$\Theta = IE\ (\%)/100 \tag{4}$$

where I_{corr}° and I_{corr} are, respectively, the current densities for the blank and copolymer as CIs.

The difference in the corrosion potential (E_{corr}) for the blank and copolymer is higher than 85 mV, suggesting that the copolymer is not a mixed-type corrosion inhibitor. The copolymer is able to decrease the current density (I_{corr}) from 180.70 to 28.39 $\mu A/cm^2$, showing 84% inhibition efficiency at a concentration of 100 ppm. In addition, the polarization resistance measured on the steel surface after injecting the copolymer increases by a factor of six, demonstrating the effective corrosion inhibition of the copolymer. Both electrochemical tests (LPT and PDP) demonstrated that the corrosion inhibition efficacy of the copolymer was greater than 84%.

Figure 3. LPR of the copolymer at 60 °C. (A) Corrosion rate versus time in the presence of the copolymer (at 50 ppm) injected at indicated times. (B) Corrosion inhibition efficiency of the copolymer calculated from the corrosion rate plot.
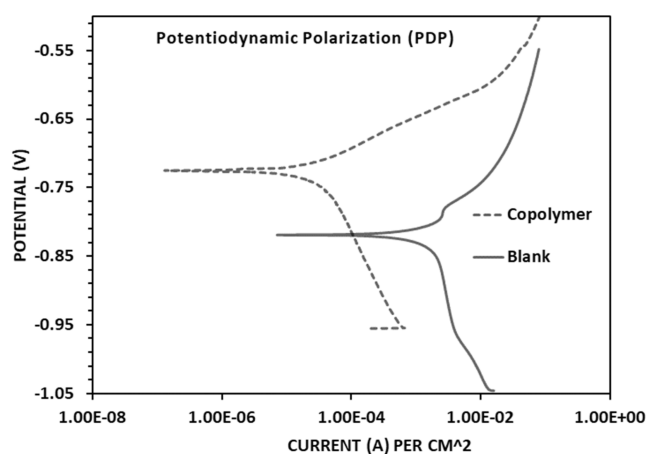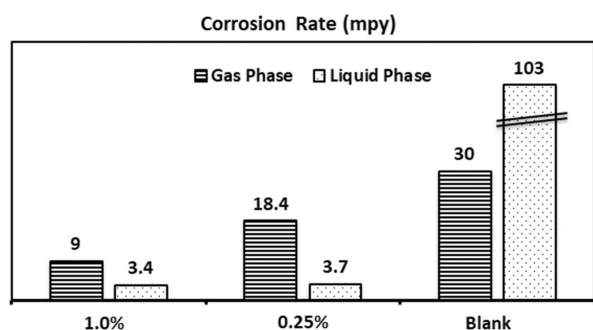
Table 6. Potentiodynamic Polarization Parameters Calculated Using Tafel Plots in Brine with and without the Copolymer

sample	E_{corr} mV	I_{corr} $\mu A/cm^2$	βa mV	βc mV	Rp (k$\Omega \cdot cm^2$)	Cr mpy	CR (mm/yr)	IE (%)	θ
blank	−819.14	180.70	52.53	128.4	89.69	87.84	2.23		
copolymer	−725.23	28.39	51.22	175.9	607.66	1.44	0.04	84%	0.84

Figure 5. Corrosion inhibition rate (mpy) in gas and liquid phases under different concentrations of the KHCI formulation using field-simulated conditions for test-1 for gas production.

3.3.3. Field-Simulated Conditions for Gas Production (Test-1).

Autoclave testing was carried out to assess the corrosion inhibition efficiency of the KHCI under field-simulated sour conditions (Table 2) at a dosage of 0.25 and 1%. Without the inhibitor, corrosion is manifested mainly in the liquid rather than in the gas phase. Already at low dosage (0.25%), the formulation was able to reduce the corrosion rate in the liquid phase from 110 mpy to 3.7 mpy, as shown in Figure 5. Furthermore, gas-phase corrosion was reduced significantly under high dosage (1%).

To further asses CI performance, the corrosion protection in the liquid phase of the inhibitor was compared not just to the blank but also to that of a conventional KHI (Conv-KHI, product based on the copolymer of acrylamide) and a conventional corrosion inhibitor (Conv-CI, product based on alkyl pyridine benzyl quaternary ammonium salt), the latter taken at standard dosage recommended by the vendor. As is apparent from Figure 6A, the KHCI outperformed both Conv-KHI and Conv-Cl in corrosion inhibition, even at a low dosage. On the other hand, when the corrosion protection performance in the gas phase is compared (Figure 6B), the KHCI outperforms all other formulations at a higher dose (1%). The KHCI's performance at a lower dosage (0.25%)

Table 7. Autoclave Corrosion Inhibition Test Results of the KHCI, Solvent System, and Blank Sample under High TDS and Low Dosage

samples	concentration (ppm)	corrosion rate (MPY)	inhibition efficiency %
KHCI	20	9.1	43.4
KHCI	100	6.3	60.8
solvent	100	11	29.9
blank		16	

Table 8. HPHT Autoclave Corrosion Inhibition Test Results of the KHCI and Blank Under Gas Production Test-2

samples	concentration (dosage %)	corrosion rate (MPY)	inhibition efficiency %
KHCI	2500 ppm (0.25%)	18	90
MEG	2500 ppm (0.25%)	48	71
blank		167	

seemingly lags behind that of Conv-CI by 3 MPY, although a greater measurement uncertainty exists in the gas phase. These findings verified KHCI's potential as a corrosion inhibitor for liquid and gas phases under field-simulated gas production conditions.

3.3.4. Field-Simulated Conditions for Wet Sour Crude Processing.

The corrosion protection performance was also assessed for wet sour crude applications under field-simulated conditions. Without a corrosion inhibitor, the corrosion rate (CR) of C-1018 in high-TDS brine was in the range of 16 mpy under sour conditions (Table 7). This rate was an average of two runs and is based on 24 h weight loss data. No pitting was observed on any of the examined coupons. Due to the fact that this is an H_2S-dominated corrosion process, the corrosion rate is projected to decrease significantly as a result of the formation of a black semi-protective iron sulfide coating. The corrosion protection activity of the KHCI at concentrations of 20 ppm and 100 ppm was then measured. At the highest concentration of 100 ppm, the KHCI was able to deliver an
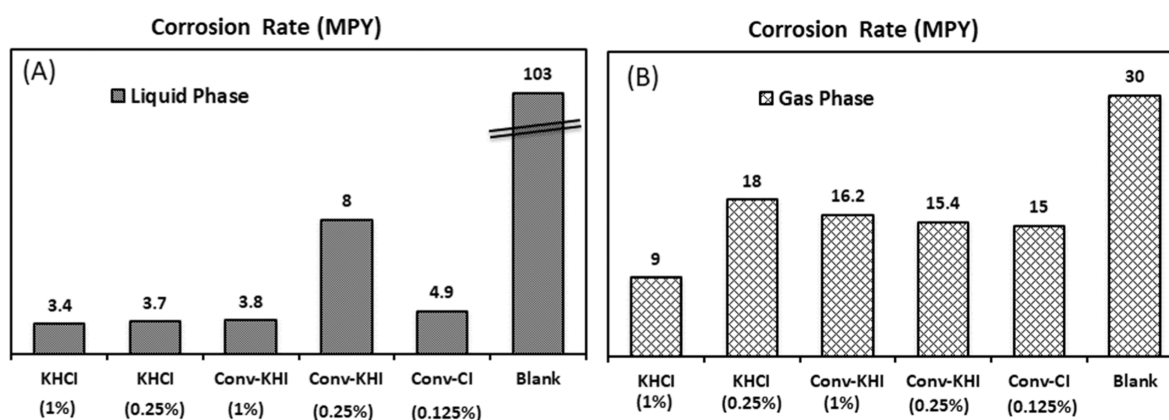
Figure 6. Corrosion rate comparison of KHCI and conventional KHI (Conv-KHI) and conventional corrosion inhibitor (Conv-CI) in the liquid phase (A) and gas phase (B) under field-simulated conditions for test-1.
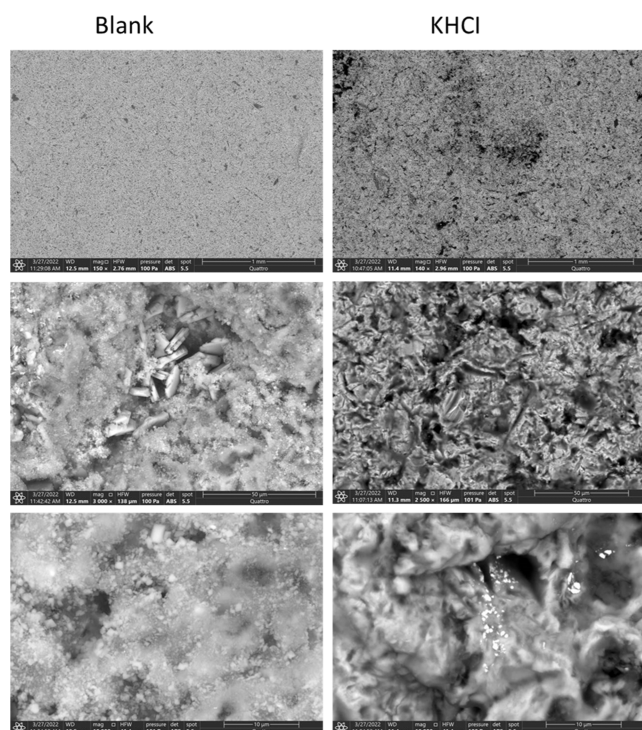
Figure 7. ESEM backscattered electron images of the corrosion film on the carbon steel coupon exposed to liquid in inhibited and uninhibited low TDS brine in sour gas at 90 °C for 42 h. Comparison of the blank sample (left column) with the KHCI (right column).

inhibition efficiency greater than 60%. Reducing the KHCI concentration to 20 ppm had a substantial effect on protection, yielding an efficiency of only 43%.

Additionally, the solvent utilized to formulate the KHCI for high TDS systems lowered the corrosion rate to 11 mpy with a 30% protection factor. The presence of certain surfactants, e.g., thiol/mercaptan, and long alkyl chain amines is hypothesized to be the cause of this protection.

3.3.5. Field-Simulated Conditions for Gas Production (Test-2). The baseline CR of the C-1018 in a low-TDS brine under sour test conditions and without corrosion inhibitor was in the range of 167 mpy (Table 8). The rate was the average of two runs based on 42 h-long weight-loss data. No pitting was observed on any of the tested coupons whether in the gas or in the liquid phase, and a thick black corrosion product coating was seen on the coupons.

A large concentration of the KHCI (2500 ppm) was necessary in this case to significantly lower the corrosion rate to 18 mpy from 167 mpy for the blank sample, providing a protection of more than 90%. The solvent (MEG) utilized to formulate the KHCI for low TDS systems seemed to already have a significant effect on corrosion protection performance.

Figure 7 shows a comparison of the ESEM images of the corrosion film on inhibited and uninhibited test coupons. The film in the blank case was loose and non-uniform with voids spread over the surface and showed a higher sulfur content, as shown in Figure 8. Conversely, the surface of the coupons tested in the KHCI showed a cleaner surface and a much lower sulfur content. The signal from carbon was observed to be high, presumably due to the presence of the inhibitor on the
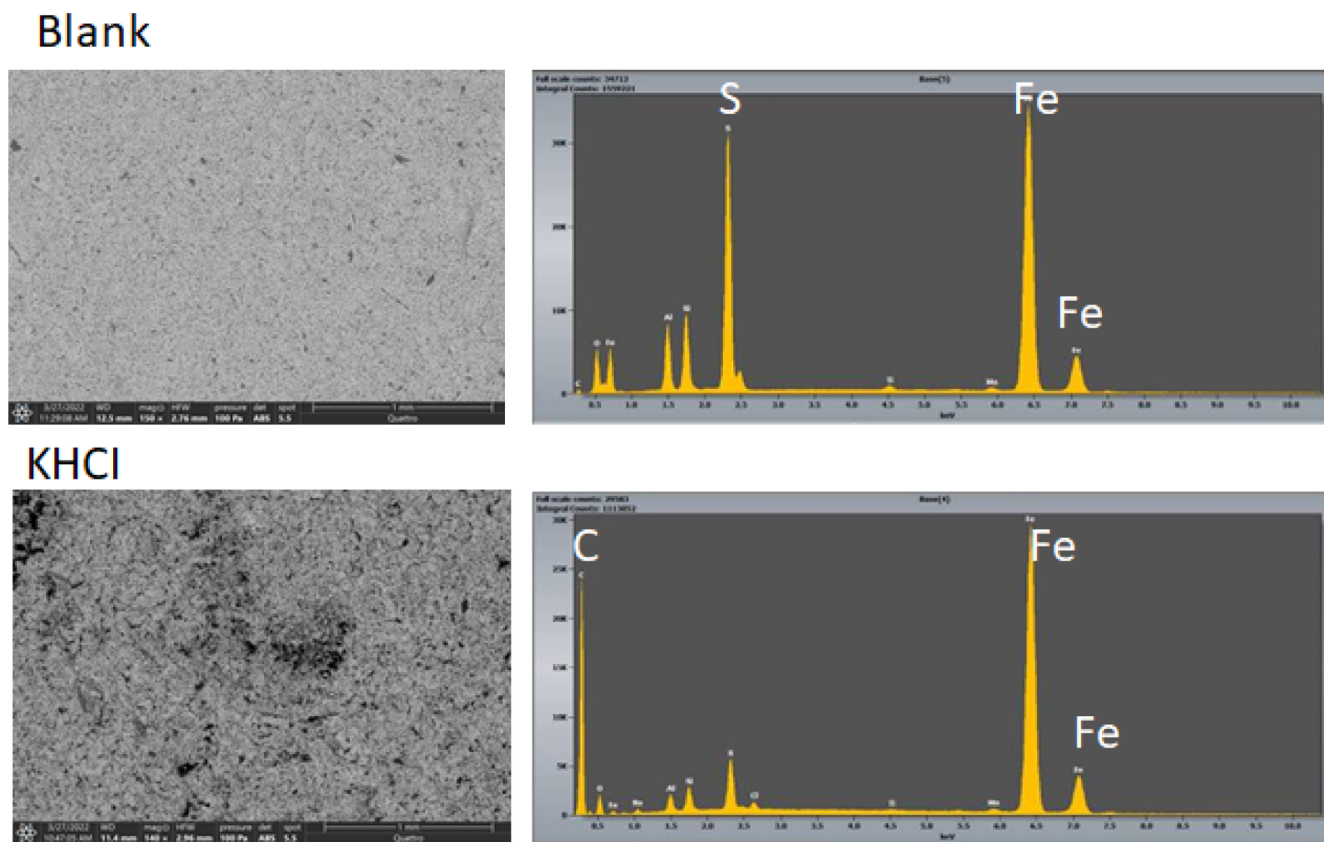

Figure 8. ESEM backscattered electron images of the corrosion film on the carbon steel coupon exposed to liquid in inhibited and uninhibited low TDS brine in sour gas at 90 °C for 42 h and EDXS spectra collected in general area mode.
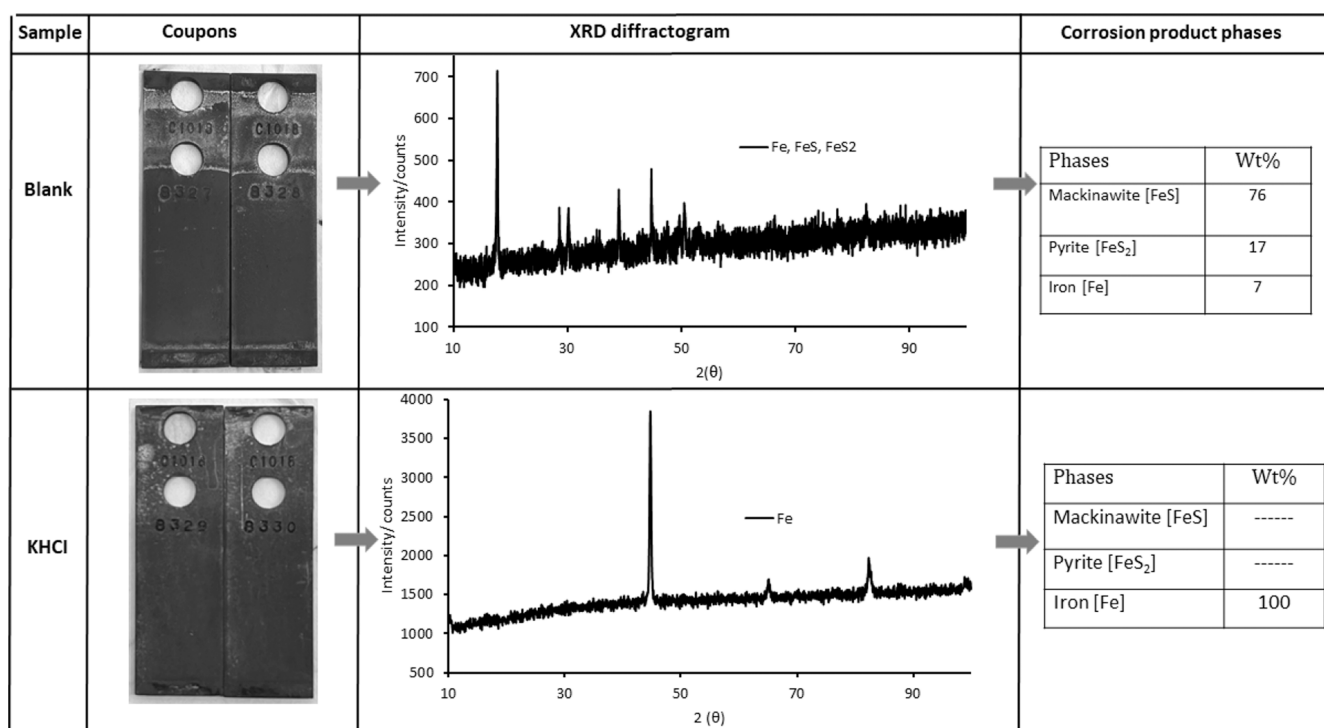
Figure 9. Images and corresponding diffractograms of the coupons and quantification of different phases of the corrosion product.

Table 9. Comparison of Inhibition Efficiencies of the Developed KHCI with Literature Data Relative to Polymeric Inhibitors for Use in CO$_2$-Saturated Brine

polymers	metal/alloys	technique used	inhibition efficiency, η (%)
gum arabic[42]	C1018 steel	LPR, PDP, and EIS	83.50 at 5000 ppm
dextran derivatives[43]	carbon steel	PDP and EIS	81.10 at 100 ppm
modified polyaspartate derivatives[44]	C1018 steel	LPR, PDP, and EIS	53.60−95.0 at 25−100 ppm
acrylamide-based terpolymer[45]	carbon steel	PDP	94.6−96.3% at 50−1000 ppm
acryloyl-based copolymer (this study)	C1018 steel	LPR and PDP	84−90 at 100 ppm

surface. General area scans and spot analyses can be seen in Figures S5 and S6 of the Supporting Information.

A quantitative composition evaluation of the coupon surface film via X-ray diffraction[41] (see Figure 9) showed the presence of the early corrosion product mackinawite (FeS) and a small quantity of pyrite (FeS$_2$) on the blank and an absence of sulfides in the other sample, in agreement with the microscopy results. The Fe identified in the diffractograms corresponded to the ferritic steel substrate, with a thick sulfide layer owing to the low intensity in the blank. More details about the peaks of the diffractogram and their matching with the database are presented in the Supporting Information (Figure S7).

3.4. Comparative Study with Literature Data of Polymeric CIs. The present work is the first on the application and testing in field conditions of a dual-purpose KHCI for wet sour crude environments. It is however also interesting to test the performance of the proposed KHCI in a more commonly available environment, such as CO$_2$-saturated brine. Focusing exclusively on polymeric inhibitors for use in
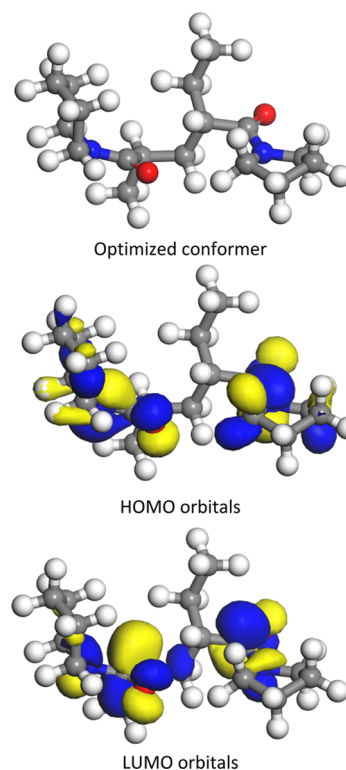

Figure 10. Optimized geometry, HOMO, and LUMO of the AB dimer in the aqueous phase.

CO$_2$-saturated brine, the literature yields only a few examples (see Table 9).

The proposed KHCI seems to perform well in CO$_2$-saturated brine, showing corrosion inhibitor performance very similar to the best previously reported formulations (modified polyaspartate derivatives).[44] Due to a lack of literature data, a
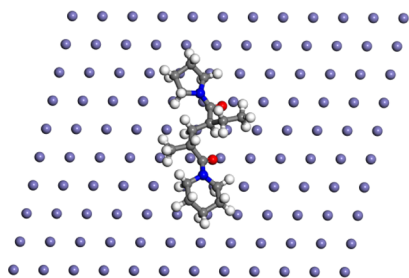
Figure 11. Snapshot (top view) of the stable adsorption configuration of the AB dimer in the aqueous phase on Fe (110). Water molecules have been removed from the image.

direct comparison of the described copolymer in a sour environment was not possible with other polymers.

3.5. Modeling and Theoretical Calculations. Figure 10 shows the optimized geometry, HOMO, and LUMO of the lowest energy conformer of the AB dimer in the aqueous phase obtained using DFT as a representative for the copolymer. The lowest energy conformer tends to have the two carbonyls on opposite sides of the chain with some minimal difference in conformational energy related to mutual orientation of the rings (armchair orientation). The HOMO and LUMO are localized on the two −CH−C≡O−N- groups of the molecule: The electron donor sites (HOMO) are available for the interaction with other molecules, whereas the electron acceptor sites (LUMO) allow for interaction with Fe (steel). The DFT also confirms that the copolymer is likely to be adsorbed on the steel surface using carbonyl groups and nitrogen. The adsorption using these heteroatoms likely forms a strong film on the steel surface and protects it against corrosive ions, leading to corrosion inhibition.

Figure 11 shows a snapshot of the stable adsorption configuration of the same AB conformer on Fe (110) in the aqueous phase. The molecule is adsorbed in a parallel orientation onto the *bcc* Fe (110) surface in accordance with the HOMO/LUMO characteristics predicted by DFT (see Figure S8 in the Supporting Information for a side view snapshot). Furthermore, the average adsorption energy obtained for the interaction is −151.3 kcal/mol, which is one order of magnitude larger than that of water (average −13.1 kcal/mol) (see Table 10). The energy spread is within kcal/mol for water and one order of magnitude larger for the short copolymer molecule, as expected due to its larger orientational space. The difference in adsorption energy between the two molecules suggests that the copolymer could displace water on the steel surface during the inhibition process. Furthermore, the high negative adsorption energy indicates spontaneous interaction between the copolymer and iron in the aqueous solution, as previously reported in the literature.[46] As a further note, the adsorption energy for the proposed copolymer is of the same order of magnitude as the one exhibited by the modified polyaspartate derivatives from the literature (Table 10). This can justify the similar corrosion

behavior exhibited by the two molecules, as previously discussed.

4. CONCLUSIONS

This work reports the corrosion inhibition properties of an acryloyl copolymer in sour environments, which had already demonstrated impressive gas hydrate inhibition. Electrochemical testing revealed the non-mixed-type nature of the CI with a corrosion inhibition efficiency of >84%, while retaining a KHI subcooling of 5.6 °C at ∼120 bars for 24 h in a sour environment. Simulated testing in a variety of field conditions showed a 60−90% corrosion inhibition efficiency at formulation dosages of 0.01−1 wt %, which was superior to a quaternary pyridinium salt-based conventional CI. Molecular modeling implicated the copolymer's heteroatoms as key to the molecule's strong adsorption onto the metal surface, with its adsorption energy on par with high-performing polyaspartate-based CIs.

Given the dearth of dual inhibitors available for sour environments, our findings pave the way for the design, development, and modification of acryloyl-based polymers to produce multiuse inhibitors that do not suffer from chemical incompatibilities.

■ ASSOCIATED CONTENT

Ⓢ Supporting Information

The Supporting Information is available free of charge at https://pubs.acs.org/doi/10.1021/acsomega.3c01290.

> Additional experimental details, IR spectrum of copolymer, NMR analysis of LCST behavior, TGA and DSC profile of copolymer, ESEM images and corresponding EDXS spectra of steel coupon surfaces, XRD diffractograms of steel coupon surfaces, and snapshot (side view) of the stable adsorption configuration (PDF)

■ AUTHOR INFORMATION

Corresponding Author

Muhammad Imran Ulhaq − *Saudi Aramco, Research and Development Center, Dhahran 31311, Saudi Arabia;* ⊙ orcid.org/0000-0003-2600-0319; Email: muhammadimran.ulhaq@aramco.com

Authors

Qasim Saleem − *Saudi Aramco, Research and Development Center, Dhahran 31311, Saudi Arabia*
Hassan Ajwad − *Saudi Aramco, Research and Development Center, Dhahran 31311, Saudi Arabia*
Rashed M. Aleisa − *Saudi Aramco, Research and Development Center, Dhahran 31311, Saudi Arabia*
Nayef M. Alanazi − *Saudi Aramco, Research and Development Center, Dhahran 31311, Saudi Arabia*
Matteo Leoni − *Saudi Aramco, Research and Development Center, Dhahran 31311, Saudi Arabia*

Table 10. Average Energy Levels for the Adsorption of the Inhibitor (Dimer) on the Fe (110) Surface in the Aqueous Phase (kcal/mol)

corrosion inhibitor	adsorption energy (inhibitor) (kcal/mol)	adsorption energy (H_2O) (kcal/mol)
acryloyl-based copolymer (this study)	−151.3	−13.1
polyaspartate derivatives- *poly(methionenaspartamide)[43]	−122.1	−12.8
polyaspartate derivatives *poly(cysteamineaspartamide)[43]	−141.4	−12.8

Ibrahim Zahrani − *Saudi Aramco, Research and Development Center, Dhahran 31311, Saudi Arabia*

Taras Makogon − *Saudi Aramco, Research and Development Center, Dhahran 31311, Saudi Arabia*

Complete contact information is available at:
https://pubs.acs.org/10.1021/acsomega.3c01290

Notes

The authors declare no competing financial interest.

■ REFERENCES

(1) Obanijesu, E.; Pareek, V.; Gubner, R.; Tade, M. Corrosion Education as a Tool for the Survival of Natural Gas Industry. *Nafta* **2010**, *61*, 541−554.

(2) Eduok, U.; Szpunar, J. Corrosion Inhibitors for Sweet Oilfield Environment (CO 2 Corrosion). *Corrosion Inhibitors in the Oil and Gas Industry*; John Wiley & Sons, Ltd, 2020; pp 177−227.

(3) Rahimi, A.; Abdouss, M.; Farhadian, A.; Guo, L.; Kaya, S.; Neshati, J. Enhancement Corrosion Resistance of Mild Steel in 15% HCl Solution by a Novel Bio-Based Polyurethane for Oil Well Acidizing. *J. Ind. Eng. Chem.* **2022**, *113*, 332−347.

(4) Ma, H.; Cheng, X.; Li, G.; Chen, S.; Quan, Z.; Zhao, S.; Niu, L. The Influence of Hydrogen Sulfide on Corrosion of Iron under Different Conditions. *Corros. Sci.* **2000**, *42*, 1669−1683.

(5) Sheng, Q.; da Silveira, K. C.; Tian, W.; Fong, C.; Maeda, N.; Gubner, R.; Wood, C. D. Simultaneous Hydrate and Corrosion Inhibition with Modified Poly(Vinyl Caprolactam) Polymers. *Energy Fuels* **2017**, *31*, 6724−6731.

(6) Lei, X.; Wang, H.; Mao, F.; Zhang, J.; Zhao, M.; Fu, A.; Feng, Y.; Macdonald, D. D. Electrochemical Behaviour of Martensitic Stainless Steel after Immersion in a H2S-Saturated Solution. *Corros. Sci.* **2018**, *131*, 164−173.

(7) Farimani, A. M.; Hassannejad, H.; Nouri, A.; Barati, A. Using Oral Penicillin as a Novel Environmentally Friendly Corrosion Inhibitor for Low Carbon Steel in an Environment Containing Hydrogen Sulfide Corrosive Gas. *J. Nat. Gas Sci. Eng.* **2020**, *77*, 103262.

(8) Javidi, M.; Haghshenas, S. M. S.; Shariat, M. H. CO2 Corrosion Behavior of Sensitized 304 and 316 Austenitic Stainless Steels in 3.5 Wt.% NaCl Solution and Presence of H2S. *Corros. Sci.* **2020**, *163*, 108230.

(9) Zhang, Q. H.; Hou, B. S.; Zhang, G. A. Inhibitive and Adsorption Behavior of Thiadiazole Derivatives on Carbon Steel Corrosion in CO2-Saturated Oilfield Produced Water: Effect of Substituent Group on Efficiency. *J. Colloid Interface Sci.* **2020**, *572*, 91−106.

(10) Davoodi, A.; Pakshir, M.; Babaiee, M.; Ebrahimi, G. R. A Comparative H2S Corrosion Study of 304L and 316L Stainless Steels in Acidic Media. *Corros. Sci.* **2011**, *53*, 399−408.

(11) Ismail, M. C.; Yahya, S.; Raja, P. B. Antagonistic Effect and Performance of CO2 Corrosion Inhibitors: Water Chemistry and Ionic Response. *J. Mol. Liq.* **2019**, *293*, 111504.

(12) Zhang, C.; Zhao, J. Effects of Pre-Corrosion on the Corrosion Inhibition Performance of Three Inhibitors on Q235 Steel in CO2/H2S Saturated Brine Solution. *Int. J. Electrochem. Sci.* **2017**, *12*, 9161−9179.

(13) Obanijesu, E. O.; Pareek, V.; Tade, M. O. *Hydrate Formation and Its Influence on Natural Gas Pipeline Internal Corrosion Rate*; OnePetro, 2010.

(14) Farhadian, A.; Varfolomeev, M. A.; Rahimi, A.; Mendgaziev, R. I.; Semenov, A. P.; Stoporev, A. S.; Vinogradova, S. S.; Karwt, R.; Kelland, M. A. Gas Hydrate and Corrosion Inhibition Performance of the Newly Synthesized Polyurethanes: Potential Dual Function Inhibitors. *Energy Fuels* **2021**, *35*, 6113−6124.

(15) Farhadian, A.; Varfolomeev, M. A.; Rezaeisadat, M.; Semenov, A. P.; Stoporev, A. S. Toward a Bio-Based Hybrid Inhibition of Gas Hydrate and Corrosion for Flow Assurance. *Energy* **2020**, *210*, 118549.

(16) Kelland, M. A. *Production Chemicals for the Oil and Gas Industry*, 2nd ed.; CRC Press: Boca Raton, 2014.

(17) Jones, R.; Morales, N.; Anthony, J.; Webber, P. A.; Harrington, R. *Development of a Novel Kinetic Hydrate Inhibitor and Corrosion Inhibitor Package for Wet Gas Application*: Rio de Janeiro, Brazil, 2013.

(18) Moore, J.; Vers, L. V.; Conrad, P. S. S. *Flow Assurance: Understanding Kinetic Hydrate Inhibitor and Corrosion Inhibitor Interactions*: Houston, TX, 2009.

(19) Makogon, T. Y.; Sloan, E. D. Mechanism of Kinetic Hydrate Inhibitors *Proceedings 4th International Conference on Gas Hydrates*; Domestic Organaizing Committee, ICGH-4: Yokohama, 2002.

(20) Moloney, J. J.; Mok, W. Y.; Gamble, C. G. *Compatible Corrosion And Kinetic Hydrate Inhibitors For Wet Sour Gas Transmission Lines*: Atlanta, GA, 2009.

(21) He, Y.; Sun, M.-T.; Chen, C.; Zhang, G.-D.; Chao, K.; Lin, Y.; Wang, F. Surfactant-Based Promotion to Gas Hydrate Formation for Energy Storage. *J. Mater. Chem. A* **2019**, *7*, 21634−21661.

(22) Clark, L. W.; Anderson, J. *Development of Effective Combined Kinetic Hydrate Inhibitor/Corrosion Inhibitor (KHI/CI) Products*: Geilo, Norway, 2006; p 14.

(23) Long, Z.; Lu, Z.; Ding, Q.; Zhou, X.; Lei, J.; Liang, D. Evaluation of Kinetic Inhibition of Methane Hydrate Formation by a Copolymer of N-Vinylcaprolactam with 1-Vinylimidazole. *Energy Fuels* **2019**, *33*, 10133−10142.

(24) Park, J.; Kim, H.; Sheng, Q.; Wood, C. D.; Seo, Y. Kinetic Hydrate Inhibition Performance of Poly(Vinyl Caprolactam) Modified with Corrosion Inhibitor Groups. *Energy Fuels* **2017**, *31*, 9363−9373.

(25) Pavelyev, R. S.; Zaripova, Y. F.; Yarkovoi, V. V.; Vinogradova, S. S.; Razhabov, S.; Khayarov, K. R.; Nazarychev, S. A.; Stoporev, A. S.; Mendgaziev, R. I.; Semenov, A. P.; Valiullin, L. R.; Varfolomeev, M. A.; Kelland, M. A. Performance of Waterborne Polyurethanes in Inhibition of Gas Hydrate Formation and Corrosion: Influence of Hydrophobic Fragments. *Molecules* **2020**, *25*, 5664.

(26) Farhadian, A.; Varfolomeev, M. A.; Shaabani, A.; Nasiri, S.; Vakhitov, I.; Zaripova, Y. F.; Yarkovoi, V. V.; Sukhov, A. V. Sulfonated Chitosan as Green and High Cloud Point Kinetic Methane Hydrate and Corrosion Inhibitor: Experimental and Theoretical Studies. *Carbohydr. Polym.* **2020**, *236*, 116035.

(27) Ulhaq, M. I. Dual-Purpose Kinetic Hydrate and Corrosion Inhibitors. *Polymeric Corrosion Inhibitors for Greening the Chemical and Petrochemical Industry*; John Wiley & Sons, Ltd, 2022; pp 161−191.

(28) Qasim, A.; Khan, M. S.; Lal, B.; Shariff, A. M. A Perspective on Dual Purpose Gas Hydrate and Corrosion Inhibitors for Flow Assurance. *J. Pet. Sci. Eng.* **2019**, *183*, 106418.

(29) Farhadian, A.; Zhao, Y.; Naeiji, P.; Rahimi, A.; Berisha, A.; Zhang, L.; Rizi, Z. T.; Iravani, D.; Zhao, J. Simultaneous Inhibition of Natural Gas Hydrate Formation and CO2/H2S Corrosion for Flow Assurance inside the Oil and Gas Pipelines. *Energy* **2023**, *269*, 126797.

(30) Gainullin, S. E.; Farhadian, A.; Kazakova, P. Y.; Semenov, M. E.; Chirkova, Y. F.; Heydari, A.; Pavelyev, R. S.; Varfolomeev, M. A. Novel Amino Acid Derivatives for Efficient Methane Solidification

Storage via Clathrate Hydrates without Foam Formation. *Energy Fuels* **2023**, *37*, 3208−3217.

(31) Omidvar, M.; Cheng, L.; Farhadian, A.; Berisha, A.; Rahimi, A.; Ning, F.; Kumar, H.; Peyvandi, K.; Nabid, M. R. Development of Highly Efficient Dual-Purpose Gas Hydrate and Corrosion Inhibitors for Flow Assurance Application: An Experimental and Computational Study. *Energy Fuels* **2023**, *37*, 1006−1021.

(32) Tang, C.; Farhadian, A.; Berisha, A.; Deyab, M. A.; Chen, J.; Iravani, D.; Rahimi, A.; Zhang, Z.; Liang, D. Novel Biosurfactants for Effective Inhibition of Gas Hydrate Agglomeration and Corrosion in Offshore Oil and Gas Pipelines. *ACS Sustain. Chem. Eng.* **2023**, *11*, 353−367.

(33) Farhadian, A.; Go, W.; Yun, S.; Rahimi, A.; Reza Nabid, M.; Iravani, D.; Seo, Y. Efficient Dual-Function Inhibitors for Prevention of Gas Hydrate Formation and CO2/H2S Corrosion inside Oil and Gas Pipelines. *Chem. Eng. J.* **2022**, *431*, 134098.

(34) Farhadian, A.; Varfolomeev, M. A.; Semenov, A. P.; Mendgaziev, R. I.; Stoporev, A. S. Dual-Function Synergists Based on Glucose and Sucrose for Gas Hydrate and Corrosion Inhibition. *Energy Fuels* **2020**, *34*, 13717−13727.

(35) Elanany, M.; Al-Malki, A.; Al-Eid, M.; Al-Daous, M.; Ali, S. A.; Majnouni, K. Acryloyl-Based Copolymers, Terpolymers, and Use as Hydrate Inhibitors. U.S. Patent 11,059,926 B2, July 13, 2021. https://patents.google.com/patent/US11059926B2/en (accessed on 2022-04-23).

(36) Ulhaq, M. I.; Al-Eid, M.; Al-Malki, A.; Elanany, M.; Ali, S. A.; Ajwad, H. A.; Saleem, Q.; Panda, S. K.; Alawani, N. A. Synthesis and Evaluation of a New Acryloyl-Based Copolymer as Kinetic Hydrate Inhibitor for Sour Gas Environments. *Energy Fuels* **2020**, *34*, 13580−13587.

(37) Imran, M.; Saleem, Q.; Ajwad, H. A.; Makogon, T. Y.; Ali, S. A.; Rushaid, A.; Panda, S. K.; Al-Eid, M.; Alawani, N. A.; Aleisa, R. M.; Jabran, A. A.; Elanany, M. Design and Development of N-Vinylcaprolactam Copolymers as Kinetic Hydrate Inhibitors for Sour Gas Environments. *Fuel* **2022**, *311*, 122497.

(38) Akkermans, R. L. C.; Spenley, N. A.; Robertson, S. H. Monte Carlo Methods in Materials Studio. *Mol. Simul.* **2013**, *39*, 1153−1164.

(39) Verma, C.; Olasunkanmi, L. O.; Ebenso, E. E.; Quraishi, M. A.; Obot, I. B. Adsorption Behavior of Glucosamine-Based, Pyrimidine-Fused Heterocycles as Green Corrosion Inhibitors for Mild Steel: Experimental and Theoretical Studies. *J. Phys. Chem. C* **2016**, *120*, 11598−11611.

(40) Lucht, N.; Eggers, S.; Abetz, V. Cononsolvency in the 'Drunken' State: The Thermoresponsiveness of a New Acrylamide Copolymer in Water−Alcohol Mixtures. *Polym. Chem.* **2017**, *8*, 1196−1205.

(41) Kaduk, J. A.; Billinge, S. J. L.; Dinnebier, R. E.; Henderson, N.; Madsen, I.; Černý, R.; Leoni, M.; Lutterotti, L.; Thakral, S.; Chateigner, D. Powder Diffraction. *Nat. Rev. Methods Primer* **2021**, *1*, 77.

(42) Shen, C.; Alvarez, V.; Koenig, J. D. B.; Luo, J.-L. Gum Arabic as Corrosion Inhibitor in the Oil Industry: Experimental and Theoretical Studies. *Corros. Eng. Sci. Technol.* **2019**, *54*, 444−454.

(43) Zhang, Q. H.; Hou, B. S.; Li, Y. Y.; Zhu, G. Y.; Lei, Y.; Wang, X.; Liu, H. F.; Zhang, G. A. Dextran Derivatives as Highly Efficient Green Corrosion Inhibitors for Carbon Steel in CO2-Saturated Oilfield Produced Water: Experimental and Theoretical Approaches. *Chem. Eng. J.* **2021**, *424*, 130519.

(44) Obot, I. B.; Ul-Haq, M. I.; Sorour, A. A.; Alanazi, N. M.; Al-Abeedi, T. M.; Ali, S. A.; Al-Muallem, H. A. Modified-Polyaspartic Acid Derivatives as Effective Corrosion Inhibitor for C1018 Steel in 3.5% NaCl Saturated CO2 Brine Solution. *J. Taiwan Inst. Chem. Eng.* **2022**, *135*, 104393.

(45) Kelland, M. A.; Pomicpic, J.; Ghosh, R.; Undheim, C.; Hemmingsen, T. H.; Zhang, Q.; Varfolomeev, M. A.; Pavelyev, R. S.; Vinogradova, S. S. Multi-Functional Oilfield Production Chemicals: Maleic-Based Polymers for Gas Hydrate and Corrosion Inhibition. *IOP Conf. Ser. Mater. Sci. Eng.* **2021**, *1201*, 012081.

(46) Verma, C.; Lgaz, H.; Verma, D. K.; Ebenso, E. E.; Bahadur, I.; Quraishi, M. A. Molecular Dynamics and Monte Carlo Simulations as Powerful Tools for Study of Interfacial Adsorption Behavior of Corrosion Inhibitors in Aqueous Phase: A Review. *J. Mol. Liq.* **2018**, *260*, 99−120.